Static, fatigue and hygroscopic performance of steel-reinforced resins under various temperatures

Christoforidou, Angeliki; Verleg, Ron; Pavlovic, Marko

DOI
10.1016/j.conbuildmat.2023.133079

Publication date
2023

Document Version
Final published version

Published in
Construction and Building Materials

Citation (APA)
Christoforidou, A., Verleg, R., & Pavlovic, M. (2023). Static, fatigue and hygroscopic performance of steel-reinforced resins under various temperatures. *Construction and Building Materials*, *403*, Article 133079. https://doi.org/10.1016/j.conbuildmat.2023.133079

Construction and Building Materials 403 (2023) 133079

Contents lists available at ScienceDirect

Construction and Building Materials

journal homepage: www.elsevier.com/locate/conbuildmat

Static, fatigue and hygroscopic performance of steel-reinforced resins under various temperatures

Angeliki Christoforidou [a], Ron Verleg [b], Marko Pavlovic [a,*]

[a] Delft University of Technology, Stevinweg 1, 2628CN Delft, the Netherlands
[b] AOC Resins, Ceintuurbaan 5, 8022AW Zwolle, the Netherlands

ARTICLE INFO

Keywords:
Steel-reinforced resin (SRR)
Polymer matrix composite
Indirect tensile spitting tests
Indirect tensile modulus tests
Indirect tensile fatigue tests
Water absorption

ABSTRACT

Resins are essential structural materials predominantly used in load-bearing connections such as adhesively bonded joints and resin-injected bolted connections. In an effort to improve the latter, a new injection material, Steel Reinforced Resin (SRR), has been developed, consisting of spherical steel particles embedded in a resin. SRR's applicability has been explored in injection bolts used in composite steel-to-concrete floor systems and as an injection material in Fibre Reinforced Polymer (FRP) sandwich web-core panels of highway bridges. While the short-term and creep performance of SRR has been researched, its fatigue behaviour remains unexplored. From joint-level cyclic experiments with SRR, it was observed that joint endurance is dominated by SRR's fatigue performance. There is currently no research on the influence of temperature on SRR's mechanical properties and moisture uptake. This paper fills this gap, by investigating the static and fatigue performance of epoxy, unsaturated polyester polyurethane hybrid (UPE + PU), and vinyl ester based SRRs under ambient and elevated temperatures. Water absorption assessments were conducted on the three resins with and without steel particles to evaluate their durability and corrosion resistance. The results show that temperature significantly impacts tensile stiffness, tensile splitting strength, and fatigue life. Epoxy based SRR endured 20 times more tensile splitting stress cycles to failure compared to the UPE + PU resin based SRR at the same stress range. However, after 200 days of water exposure at maximum temperature, the epoxy resin (with and without steel shot) exhibited a weight increase of 4.0% and 0.50% respectively, suggesting that despite its superior fatigue performance, it may not be suitable for SRR applications in high moisture environments. In contrast, UPE + PU resin and its corresponding SRR displayed substantially lower water absorption.

1. Introduction

In engineering practice, resins are essentially used either as a thick structural bonding layer conversely to the traditional mechanical joining techniques or as an injected substance for bolts, studs, and void fillings. Additionally, polymeric materials are one of the two main ingredients to make fibrous composites. Many of these structural applications, such as in bridge construction, have to undergo a high number of fatigue cycles due to fluctuating loads. In that respect, extensive research on adhesive joints or Fibre Reinforced Polymer (FRP) coupons has been conducted.

However, the influence of joint configuration on adhesives' stress state response [1] and the role of polymer matrices in composites' fatigue behaviour [2,3] has prompted increasing interest in investigating the fatigue resistance of bulk adhesive coupons [4]. Consequently, research dating back to the 1960s revealed that the crack initiation and propagation rates differ among the various types of resins, resulting in significant fatigue life variations [5]. Beyond the influence of resin type, a dependency on fatigue endurance was demonstrated by alternating the testing frequency, the magnitude of cyclic load, the R ratio, and the environmental effects [6].

One key discovery was the inverse relationship between the fatigue life of resins and testing frequency. More specifically, increasing the frequency results in elevated temperature levels within the resin, ultimately degrading its mechanical properties [6,7] and impairing fatigue performance. Regarding the R ratio, it has been proved that the slope of the S-N curve is steeper for reversed loading than for tensile-tensile or compression-compression fatigue loadings [8].

In addition to these factors, environmental conditions represent another important parameter in the fatigue behaviour of resins. Despite resins often being shielded from detrimental external influences in most

* Corresponding author.
E-mail address: m.pavlovic@tudelft.nl (M. Pavlovic).

https://doi.org/10.1016/j.conbuildmat.2023.133079
Received 24 April 2023; Received in revised form 17 July 2023; Accepted 20 August 2023
Available online 31 August 2023

applications, the long operation lifetime means it cannot be guaranteed that the resins will not be exposed to moisture or even water. Their high sensitivity to temperature is another concern, as their material properties tend to degrade owing to thermal effects such as softening [9,10]. Recent studies have demonstrated the significant influence of environmental conditions, such as immersion in tap water and seawater, as well as associated thermal effects, on the mechanical properties of epoxy resins [11,12]. From fatigue experiments conducted on aged and unaged coupons, it was observed that exposure to water induced plasticization and softening of the material [13]. Thus, the slopes of the S-N curves were, yet again, greatly increased, indicating a detrimental effect on the material's fatigue performance.

Aiming to improve the durability of the resins, polymer matrix composite materials were invented. In particular, several researchers suggested modifications to the resin's composition by introducing various inclusions. Among these alterations, the incorporation of carbon nanofibers into the bulk resin system has received widespread attention due to its potential to enhance the mechanical and thermal properties, as well as fracture toughness, of the resulting composite material [14]. Later it was proved beneficial also in terms of durability and fatigue resistance [15]. Apart from randomly shaped fillers, nano, and microspherical particles are also used as reinforcement [16]. In particular, a swift of the S-N curve with higher fatigue lifetime and the same slope was reported in the polymers with rubber and silica nanoparticles [17]. Besides the nano or micro inclusions, Nijgh [18] proposed reinforcing commercially available resins using macro steel particles i.e., steel balls of a few millimetres in diameter. The steel particles were selected for their easy workability, immediate availability, and cost-effectiveness. More importantly, they have been demonstrated to enhance the stiffness and creep resistance of the resulting composite material [18]. However, up until now, there is no literature available on the fatigue performance and water resistance of such steel-reinforced resins (SRRs).

Initially, this new type of resin reinforced with steel particles was investigated as an injection material for composite floor systems using an epoxy resin system [19]. In following studies, SRR was employed as a cavity filler in FRP decks for highway bridges applying an unsaturated polyester polyurethane hybrid system [20,21], henceforth indicated as UPE + PU. However, despite the successful application of SRRs in various structures, so far there is no information on their performance under diverse environmental conditions. Nonetheless, a compilation of material properties at room temperature has been made available and is presented in Table 1. The results indicate that material properties are subject to variation depending on factors such as the resin composition (epoxy or UPE + PE), type of hardener (HY 2440 or HY 5159), the geometry of the test specimens (diameter and length of coupon cylinders), or the percentage of steel shot (60% or 80%). This suggests the need for careful optimization of these parameters when creating composite SRR materials.

Concerning the cyclic performance of SRR material, previous experiments focused only on a connection level [20]. However, in a recent publication, it has been suggested that the fatigue performance of these connections is predominantly dictated by the stresses experienced within the SRR component [22]. Hence, there's an imperative need to examine the fatigue response of the SRR material itself, particularly its susceptibility to varying environmental conditions.

Therefore, the primary objective of this study is to address the aforementioned gaps by evaluating the performance of various SRR types. The focus is on application-oriented requirements such as resistance to cyclic loading and environmental conditions, like moisture and increased temperature. Through a series of tests, the static mechanical properties and fatigue performance of SRR material will be assessed at both ambient and elevated temperatures. The aim of this study is to present a comprehensive understanding of the performance of various SRRs under a spectrum of conditions, thereby providing valuable insights for their optimal use in engineering applications.

The paper is structured as follows. In Section 2, an evaluation of the tensile properties of three distinct types of SRRs at both room and elevated temperatures using indirect tensile splitting test configurations is presented. In Section 3, the focus shifts to the fatigue performance of these materials. Initial stress-cycle (σ-N) diagrams from indirect tensile fatigue tests conducted at ambient temperature are presented, supplemented with additional fatigue experiments at elevated temperatures. Section 4 assesses the long-term practicality of SRR materials by examining their susceptibility to aging. This involves conducting water absorption tests on all three resin compositions, considering scenarios both with and without the inclusion of steel balls. Finally, in Section 5 a consolidation of the main points and an elaboration of the key findings of this study are provided.

Table 1
Collection of mechanical properties of SRR at room temperature from literature.

Type of SRR	Property	Methodology	
40% epoxy, RenGel SW 404 + HY 2404 60% steel shot	E = 15.7 GPa	5 compression tests on unconfined specimens D26,3x50 mm	[23]
	fu = 120.3 MPa	5 compression tests on unconfined specimens D26,3x50 mm	[23]
	v = 0.22	1 compression test on unconfined specimens D26,3x50 mm	[23]
	v = 0.19	Numerically determined	[19]
	E*=17.6 GPa *: Apparent Young's modulus	5 compression tests on unconfined specimens D22x22 mm	[19]
40% epoxy resin, RenGel SW 404 + HY 5159 60% steel shot	E = 21.9 GPa	3 compression tests on unconfined specimens D22x22 mm	[24]
	f_c = 136.2 MPa	3 compression tests on unconfined specimens D22x22 mm	[24]
	v = 0.22	Assumed based on a test with another hardener HY 2404	[24]
	v = 0.20	Numerically determined	[19]
20% UPE + PU, Daron 8150 80% steel shot	E = 9.3 GPa	3 compression tests on unconfined cylinders D62x130 mm	[25]
	f_c = 74.3 MPa	3 compression tests on unconfined cylinders D62x130 mm	[25]
	f_t = 10.1 MPa	3 tensile splitting tests on unconfined cylinders D62x130 mm	[25]

2. Tensile properties of SRR at room and elevated temperatures

In this section, an overview of the experimental investigation conducted to evaluate the mechanical properties; specifically, indirect tensile strength, stiffness, and Poisson ratio, of three distinct SRR compositions is presented. Three different groups of SRR coupons were produced solely dependent on the applied resin systems, which are described in the subsequent section. The mechanical properties of the SRR were derived from cylindrical coupons subjected to indirect tensile loading. This testing approach, commonly referred to as the Brazilian test in the literature, is widely adopted for granular materials such as asphalt [26], concrete mixtures, rocks, or even soil.

2.1. Resin systems considered

Epoxy resins are widely used due to their excellent mechanical properties, versatility, low shrinkage on curing, and ease of use. However, their high viscosity has led to challenges in molding and injection processes, prompting interest in alternative resin types such as vinyl ester or polyurethane resins. Vinyl ester resins, with their low hydrophobic features, have demonstrated superior hydrothermal aging

resistance compared to epoxies [27]. With regard to polyurethane resins, although they have been used in various structural applications due to their versatile properties, certain types with a weak elastomeric nature and high thermal expansion coefficient were initially deemed unsuitable for larger structural forms [28]. The introduction of unsaturated polyester as an additional reactive polymer led to the development of UPE + PU, effectively eliminating the deficits of polyurethane resin [29].

Three resin systems appertain to the main categories described above were investigated. More specifically, an infusion epoxy resin commercially available as Resoltech 1080S/ Hardener 1083, the vinyl ester resin Atlac 430LV and the UPE + PU resin called AQR 1025/B25 were considered in this work. The main characteristic that all three have in common is their high glass transition temperature ($T_g > 100$ °C) when subjected to complete curing conditions. This information together with their Young's modulus (E), maximum tensile strength (f_u), and viscosity (η) at 23 °C are reported in Table 2 as provided by the resin suppliers [30–32].

2.2. Resin preparation and production of specimens

All resins were prepared at room temperature, adhering to the supplier-recommended mixing ratios [30–32]. The epoxy resin was created using a 100/20 mixing ratio between the Resoltech 1080S and the Hardener 1083, respectively. For the UPE + PU resin, a three-component resin, 2 g of a catalyst system, supplied as PerkadoxCH50, were dissolved into 100 g of Daron 8151 (2% wt) followed by the addition of 25 g of Lupranate M20R + 29 after thorough stirring. Lastly, the Vinyl ester resin was prepared by mixing 100 g of Atlac 430LV and 2 g of PerkadoxCH50, representing 2% of the Atlac 430LV weight. Each mixture was stirred for at least 1 min to ensure proper dissolution.

Steel-reinforced resin discs were produced by mixing the steel shot with the resin and placing the mixture in an acrylic cylindrical mold. All the coupons were manufactured with equal proportions of both ingredients i.e., 830 gr of steel shot and 65 gr of resin. This ratio yielded an average thickness of 23 mm for the SRR specimens while the diameter was set to 100 mm. To avoid the formation of air bubbles due to mixing, the specimens were placed on a vibrating table for five minutes. Following a one-day curing period at ambient temperature, the samples were post-cured at 60 °C for five hours as specified in [30].

2.3. Description of experiments

Depending on the specific mechanical property under investigation, varying loading protocols and instrumentation were employed. These are further detailed in Table 3. For the investigation of strength and Poisson ratio, the force was applied using a 50 kN MTS actuator and measured with a Lebow 50 kN load cell. This actuator was managed by an Instron test controller, featuring a frequency range of 0.001 – 30 Hz and a strain rate range of 0.001 – 5% per second. The experimental setup was placed in a Weiss Enet temperature cabinet with internal dimensions of 1.0x1.0x1.0 m. This cabinet allows precise control of internal temperature, ranging from −40 to 60 °C, through electrical heating control with an accuracy of 0.1 °C.

When determining stiffness, a pneumatic Universal Testing Machine (UTM) was utilized, equipped with a load cell of a maximum capacity equal to 5 kN. This setup was positioned within a temperature cabinet with internal dimensions of 0.5x0.8x1.0 m, capable of sustaining a temperature range between 0 and 60 °C. Solartron linear variable displacement transducers (LVDTs) were employed to monitor the horizontal displacements during stiffness tests, offering a maximum capacity of ± 1 mm. Lastly, during the tests for determining the Poisson's ratio, a Canon EOS 5DS DSLR camera was used to capture photos of the specimen.

Table 2
Available properties of the investigated resins.

Type	Name	E [GPa]	f_u [MPa]		η [mPa.s]	$T_{g,max}$ [°C]
Post cure		Fully	5hr60 °C	Fully		Fully
Infusion epoxy	Resoltech 1080S/ Hardener 1083	2.91	77	116	1100	110
UPE + PU	AQR 1025/ B25	3.53	77	95	150 – 220	135
Vinyl ester	Atlac 430LV	3.13	67	95	440 – 500	130

2.4. Indirect tensile splitting strength of SRR at different temperatures

The heterogeneous composition of composite materials with granular additions complicates the acquirement of their tensile strength via dog-bone tensile coupons, as in bulk adhesives. Thus, the strength of the SRR material was assessed by applying compressive force in the vertical plane of cylindrical coupons, generating horizontal tensile stresses that lead to fracture. Indirect tensile splitting tests were performed at room and elevated temperatures e.g., 25 °C, 40 °C, and 55 °C, and the setup is shown in Fig. 1.

The load was applied at a constant rate of 25 mm/min using two 12 mm thick steel loading strips in contact with the disk-shaped SRR coupon. To determine the indirect tensile splitting strength the specimens were loaded until failure. A tensile crack at the centre of the discs was observed, as displayed in Fig. 1. The average force versus the recorded stroke curves from the three tests performed for each type of SRR are presented in Fig. 2. The initial straight line, observed until 0.4 mm for the case of UPE + PU, is attributed to the absence of contact between the specimen and the loading blade. Subsequently, a nonlinear section, noticeable up until approximately 10 kN of applied load arose from plotting the external force against the total displacement. The latter incorporates the settlement of the specimens in the apparatus or the localised crushing near the loading areas. This nonlinearity has also been attributed to densification in the case of asphalt concrete mixtures under indirect tensile loading [33], or to the bedding-in effect for anisotropic rocks under the indirect tensile splitting test arrangement [34].

The resulting tensile splitting stress (horizontal) $\sigma_{x,max}$ at the centre of the specimen in (MPa) was calculated using the conventional formula for homogeneous and linear elastic materials tested as outlined in [35]. In particular, the vertically applied force is divided by the corresponding tensile area as follows:

$$\sigma_{x,max} = \frac{2 \bullet F}{\pi \bullet D \bullet t} \quad (1)$$

where F represents the vertically applied loading (N); D is the diameter of the test specimen (mm); and t is the thickness of the test specimen (mm).

The results of the tensile strengths of the three types of resins under varying temperatures are shown in Table 4. The maximum strength was observed for the SRR produced with epoxy resin at room temperature, equating to 11.6 MPa which diminished by 13% and 22% once temperature rose to 40 °C and 55 °C, accordingly. For the Vinyl ester based SRR, the ultimate tensile strength of the coupon was not affected by temperature changes. However, it consistently exhibited the lowest strength value, approximately 6.8 MPa, across all three temperature conditions. Regarding the UPE + PU based SRR specimens, the 10 MPa tensile strength at room temperature aligns with the tabulated results in Table 1, reported in literature [25]. The strength reduction due to temperature increase follows a similar trend to that observed for the epoxy resin, as depicted in Fig. 3. Lastly, under the same post-curing conditions, the addition of steel reinforcement in the pure resin matrix

Table 3
Description of experiments for determining mechanical properties.

Property	Loading	Instrumentation	Temperatures	Coupons[1]	Machine
Strength	25 mm/min	Machine	25, 40, 55 °C	3	MTS-50
Stiffness	5 compressive pulses	LVDTs	25, 40, 55 °C	3	UTM-5
Poisson ratio	0.01 mm/sec	Camera	25 °C	3	MTS −50

[1] Number of coupons per testing temperature.

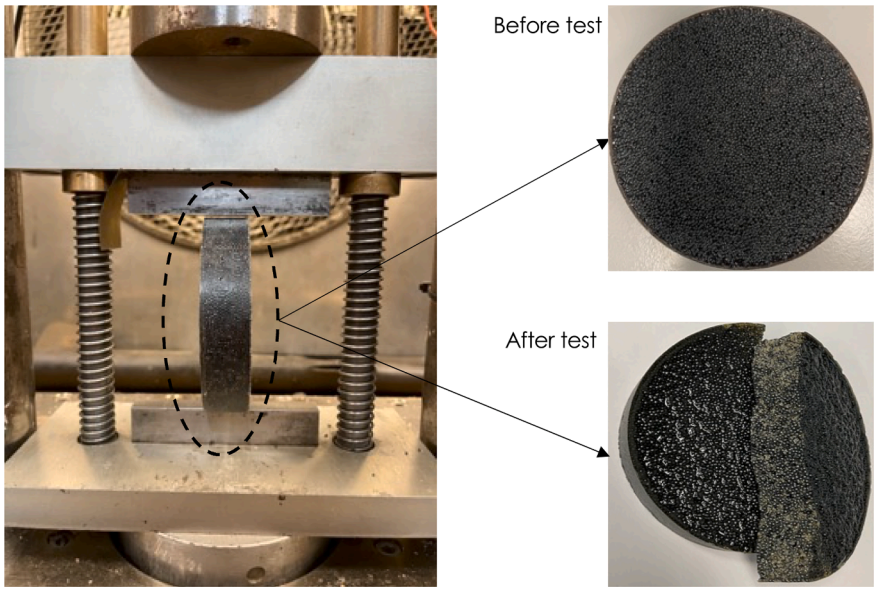

Fig. 1. Indirect tensile strength test set up and coupon prior and after testing; epoxy based SRR.

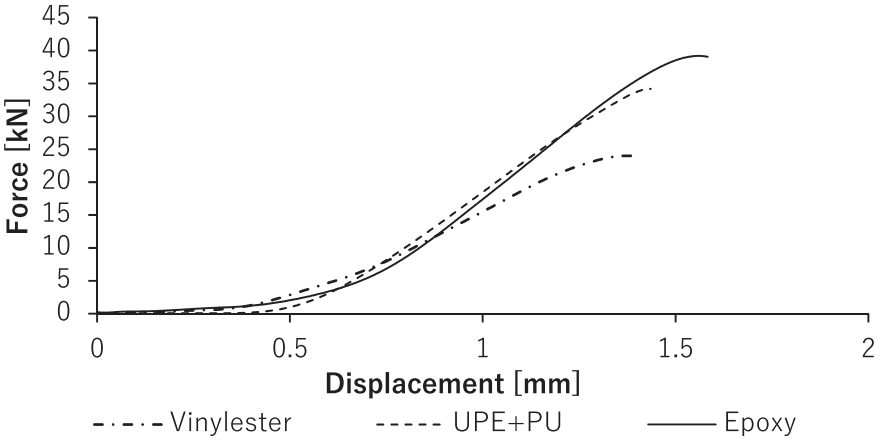

Fig. 2. Average tensile splitting force versus displacement at 25 °C from stroke of the machine.

Table 4
Average strength values for various temperatures and types of resins.

Resin	Strength at 25 °C (MPa)	Strength at 40 °C (MPa)	Strength at 55 °C (MPa)
Epoxy (COV %)	11.6 (2.7%)	10.1 (3.6%)	9.0 (2.0%)
UPE + PU (COV%)	10.0 (3.9%)	8.9 (2.2%)	7.5 (9.9%)
Vinyl ester (COV%)	6.8 (2.2%)	7.1 (8.6%)	6.6 (5.6%)

led to an approximately 85% reduction in their tensile strength, as tabulated in Table 2 and Table 4.

2.5. Poisson ratio of SRR

To accurately ascertain the indirect tensile modulus of granular materials, it is imperative to determine their Poisson ratios. In the subsequent sections, the Poisson ratios are deduced through a combination of numerical and experimental approach. Initially, the horizontal and vertical extensions will be derived, followed by the establishment of a numerical model designed to correlate the horizontal-to-vertical proportion with the material's Poisson ratio. The results presented focus on the two SRRs with the highest static strength, specifically the epoxy and

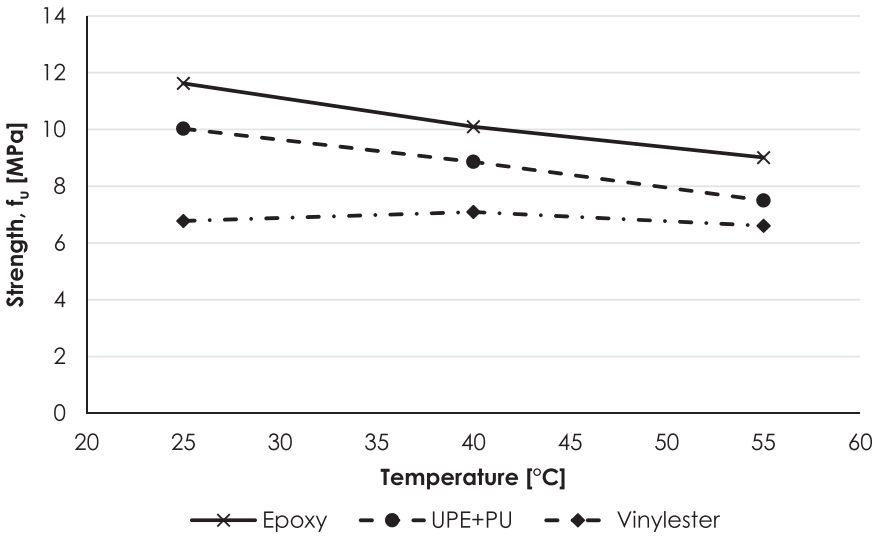

Fig. 3. Average indirect tensile splitting strength variation under various temperatures.

the UPE + PU resin systems.

2.5.1. Experimental approach

A setup analogous to the one used for the indirect tensile strength tests described in Section 2.3 was employed, with the primary difference being the incorporation of a single camera to perform the digital image correlation (DIC) technique to quantify the surface planar deformations. Sequential digital images were captured for two SRR coupons that were loaded up to 20 kN of force at a loading rate of 0.01 mm/sec. The image capture was synchronised with the load from the test frame through a data acquisition system.

A fine speckled pattern was applied to the coupons, as shown in Fig. 4**a**. From the DIC analysis performed on an SRR disk made with epoxy and UPE + PU resin, the ratio between the vertical and the horizontal strain, as depicted in Fig. 5**,** was equal to 0.1312 and 0.129, respectively. These extensions were calculated via virtual extensometers positioned at least 10 mm away from the edges and loading points to avoid local effects, as sketched in Fig. 4**b**.

2.5.2. Numerical analysis

Two-dimensional plane-stress finite element (FE) models of the complete steel-reinforced disk geometry were developed in the commercial software Abaqus/CAE 2021. The diameter and thickness of the disk were set equal to 100 and 23 mm, respectively, corresponding to the sample size used in the physical tests. The built-in 2D plane stress elements of four or three nodes (CPS4R and CPS3) from Abaqus/Standard were chosen to mesh the circular geometry (Fig. 6**a**). An approximate element size of 0.3 mm with a quad-dominated shape, an advancing front algorithm and a free technique were applied. This resulted in a total number of elements equal to 104,674 for the linear quadrilateral elements of type CPS4R and 3194 for the linear triangular elements of type CPS3.

Steel loading strips were not explicitly modeled; instead, the two contact areas of the blades were kinematically constrained i.e., coupled to the reference points (RP1, RP2), as shown in Fig. 6**b**. Displacement-controlled loading was prescribed to the reference point on the upper part of the disk, RP1 (Fig. 6**c**), with a maximum vertical displacement of 0.5 mm. Additionally, a fully fixed boundary condition was applied in the reference point RP2 in the lower part of the disk.

The purpose of the two FE models was to ascertain the correlation between the ratio of horizontal to vertical deformation and the Poisson ratio of the SRR based on two resin types. The SRR material was approximated on a *meso*-level as a linear, isotropic, and homogeneous material. Given that the FE models were exclusively utilized at this phase to establish a connection between the vertical and horizontal extensions and the Poisson ratio, a preliminary Young's modulus value

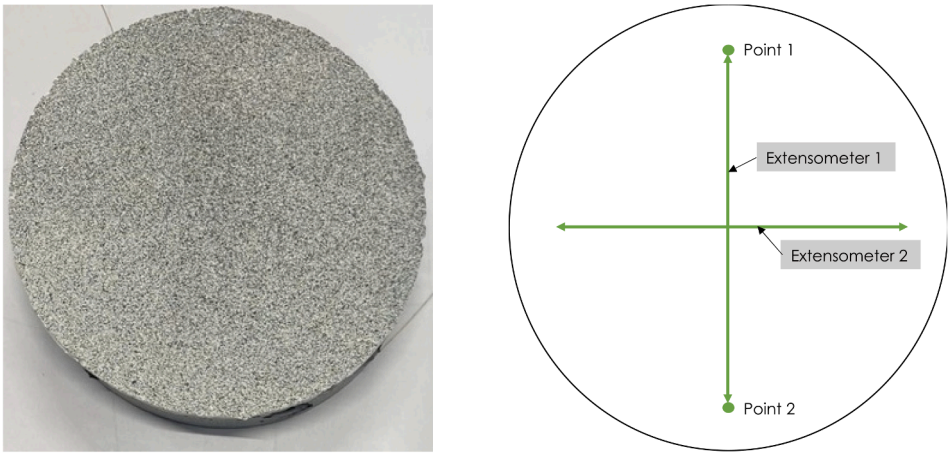

Fig. 4. DIC based displacement measurement; (a) Speckled pattern on UPE + PU based SRR disk, (b) location of virtual extensometers.

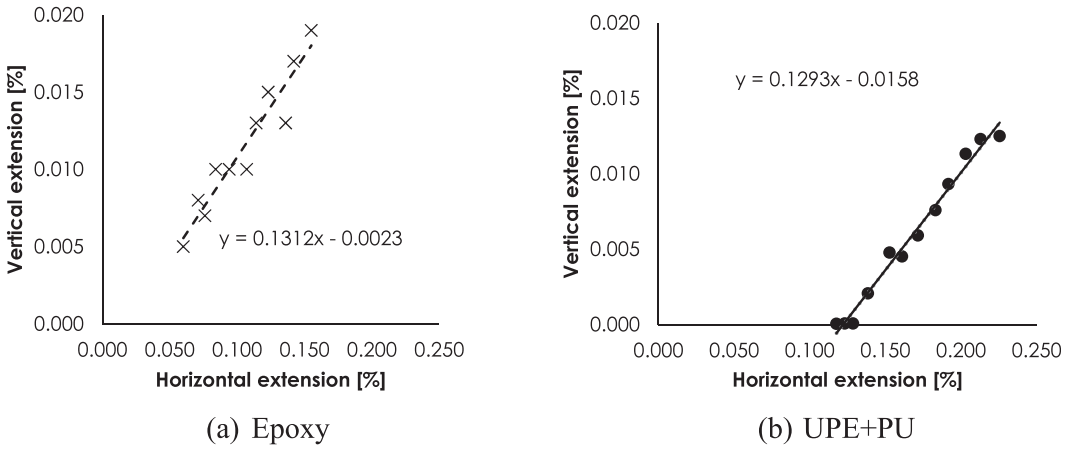

Fig. 5. Horizontal versus vertical extension from DIC of SRR coupons loaded from 5 kN until 15 kN.

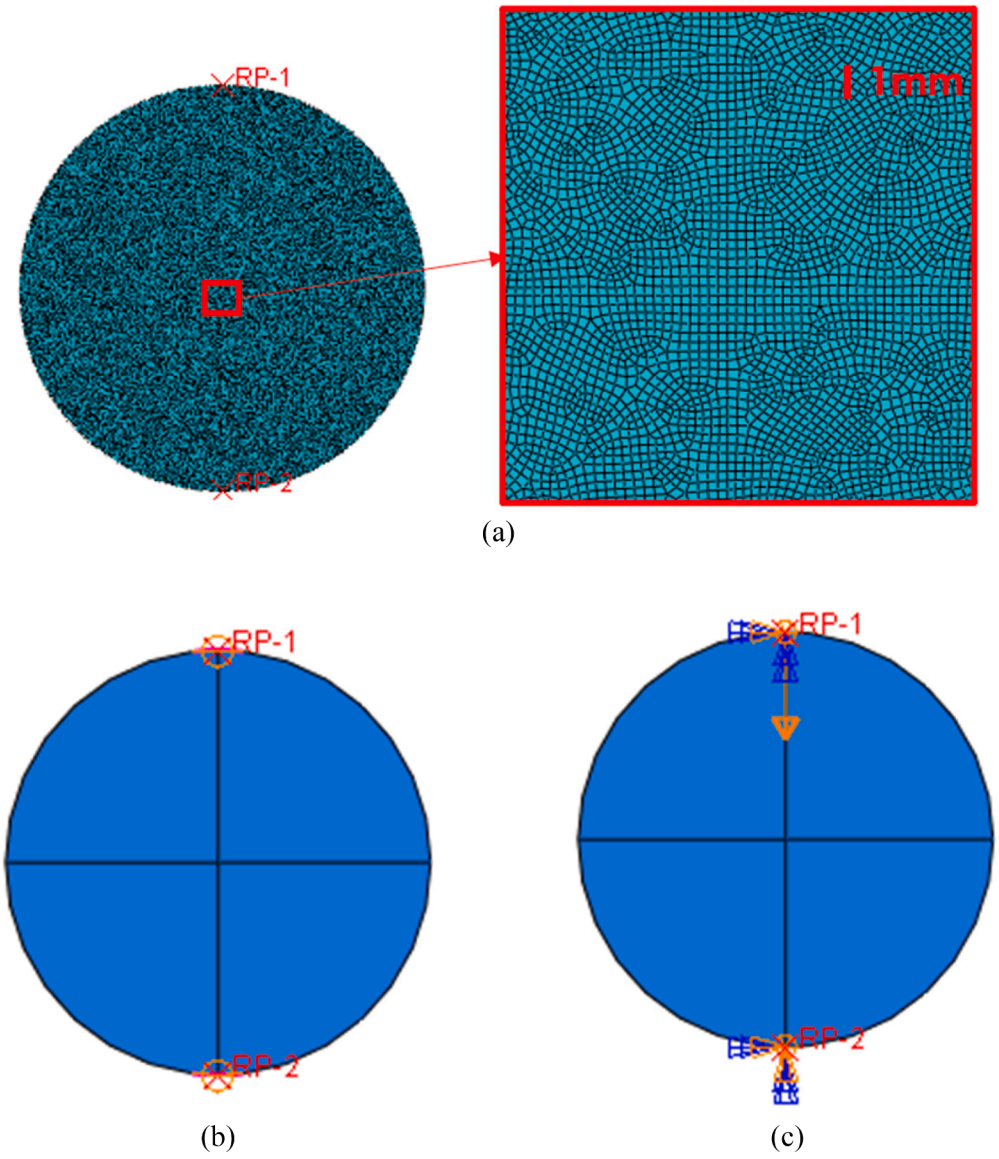

Fig. 6. Description of FE model of the disk; (a) mesh (b) reference point coupled to the arc (c) boundary conditions for the disk.

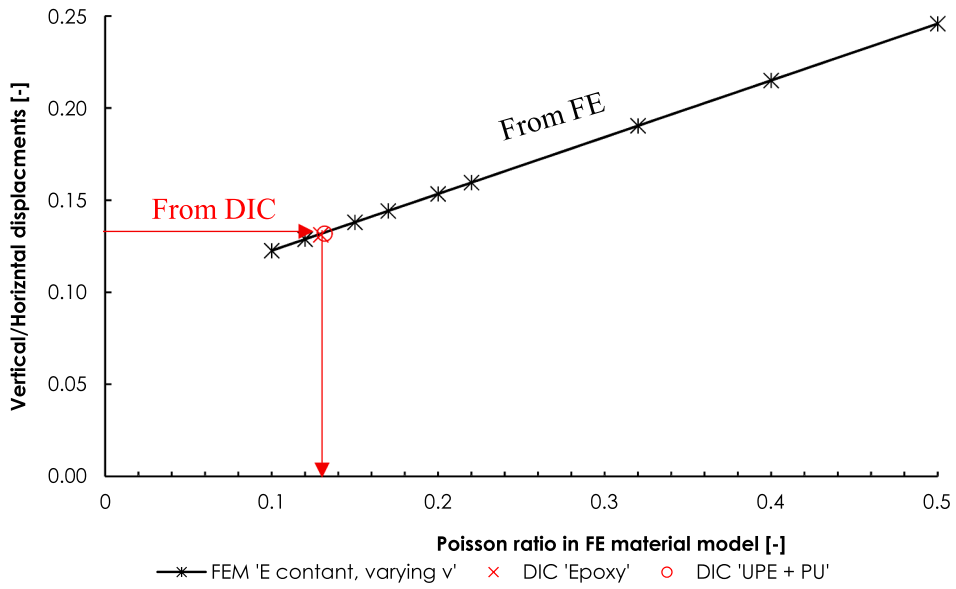

Fig. 7. Poisson ratio versus ratio between vertical and horizontal extension.

of 20 GPa was assumed, with the Poisson ratio ranging between 0.1 and 0.5.

The proportion of vertical to horizontal displacements was extracted from a series of 2D linear elastic and homogeneous material models, each exhibiting varying Poisson's ratios. Fig. 7 shows the relation between the Poisson ratio and the proportion of vertical versus horizontal extension. Based on the vertical-to-horizontal deformation ratios determined by DIC in the experiments, the Poisson ratio of 0.13 is found to be fairly similar for epoxy and UPE + PU based SRR (refer to the red markers in Fig. 7).

Fig. 8. Setup of indirect tensile stiffness modulus test.

2.6. Indirect tensile stiffness of SRR at different temperatures

A non-destructive test took place to obtain the stiffness modulus of the same SRR coupons which were used later to determine the indirect tensile strength. In accordance with [36], five compressive pulses were applied, ensuring a peak transient horizontal deformation of 5 μm gauged by LVDTs, as depicted in Fig. 8. The relationship to obtain the stiffness modulus is as follows:

$$E_t = \frac{F}{\Delta l \bullet t} \bullet (\nu + 0.27) \quad (2)$$

where F denotes the vertically applied loading (N); Δl is the peak horizontal diametral deformation (mm); t represents the thickness of the test specimen (mm); and ν is the Poisson's ratio of the SRR material.

The vertical load, measured by a load cell, ranged from 4.6 kN to 5 kN for the prescribed horizontal deformation. The experimental temperatures encompassed a range of 25, 40, and 55 °C.

Utilizing Equation (2), the stiffness modulus for the SRR based on three types of resins was calculated at three different temperatures, as tabulated in Table 5. A total of three specimens were tested for each resin type. From this table, it can be concluded that the stiffness of the UPE + PU based SRR exhibits no significant reduction in response to temperature increase from 25 °C to 40 °C. Conversely, the epoxy and vinyl ester based SRRs experienced stiffness reductions of 15% and 12% at 55 °C compared to 25 °C. The difference in the mean stiffness modulus with respect to the variation of temperatures is illustrated in Fig. 9. The stiffness of the epoxy based SRR experienced the most pronounced reduction.

2.7. Validation of elastic material properties

The determined stiffness from the splitting test is reliant on the

Table 5
Average stiffness moduli for various temperatures and types of resins.

Resin	Stiffness at 25 °C (GPa)	Stiffness at 40 °C (GPa)	Stiffness at 55 °C (GPa)
Epoxy (COV%)	16.6 (7%)	14.0 (10%)	13.1 (9%)
UPE + PU (COV%)	16.2 (6%)	16.2 (16%)	14.9 (14%)
Vinyl ester (COV%)	14.7 (4%)	12.9 (9%)	13.1 (4%)

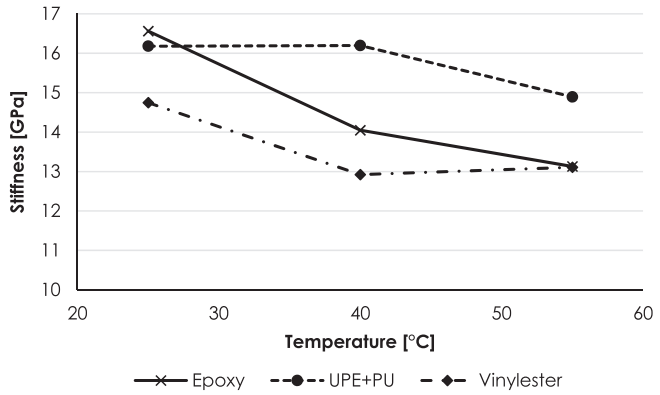

Fig. 9. Average stiffness variation under various temperatures.

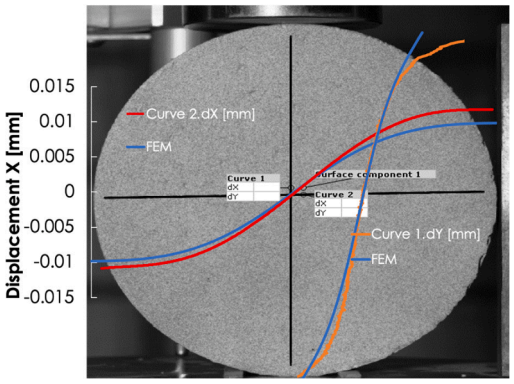

Fig. 11. Vertical and horizontal displacements along the main lines; SRR with epoxy resin at 20 kN.

Table 6
Elastic material properties for SRR with epoxy and UPE + PU resin tested at 25 °C.

Material	Stiffness [GPa]	Poisson ratio [-]
SRR with Epoxy resin @25 °C	16.6	0.13
SRR with UPE + PU resin @25 °C	16.2	0.13

Poisson ratio. To validate the selected Poisson ratio and the resulting stiffness of SRR the combination of these two elastic properties is inputted into the FE model, see Table 6. Further on the load–displacement and spatial displacements from the model are compared to DIC measurements from the experiments.

The vertical displacements from DIC, extracted 10 mm beneath the loading point and above the support, were used to compare the vertical displacements from the model and experiments excluding the local indentation effects at load introduction. The load–displacement graphs are shown in Fig. 10. It should be noted that the initial non-linear part reported in Fig. 2 is not evident in these graphs, primarily due to the fact that the DIC displacements were obtained from spatially remote points with respect to the load application points. This observation is consistent with findings reported in [37,38], where the vertical or horizontal strains were extracted from the center of the coupons using DIC.

In a more detailed analysis, the distribution of vertical and horizontal displacements across the disc specimen are compared in Fig. 11. Both load–displacement and spatial deformation results of the experiments and the models match well. This is an indirect justification that the determined combination of stiffness and Poisson rations of the epoxy and UPE + PU based SRRs are valid.

3. Cyclic response of SRR

The fatigue performance of the epoxy and UPE + PE based SRR were characterised using an experimental setup analogous to the one employed for the indirect tensile strength test. The cyclic loading was applied to SRR disk coupons of 100 mm diameter and 23 mm thickness. The fatigue endurance of the SRR disks was defined as the number of load cycles resulting in the full fracture of the specimens.

The constant load amplitude was applied to the SRR disks in a sinusoidal form with a frequency of 5 Hz (force-controlled). The load ratio, or R-value, for all specimens was maintained at 10, indicating that the specimens were subjected to compressive loading exclusively. However, this resulted in an indirect tensile splitting behaviour. Therefore, indirectly, the stress ratio R = 0.1 is applied in these tensile splitting cyclic experiments. SRR of both resin systems were tested using the same stress ranges, namely 7 MPa, 5.55 MPa, and 5 MPa. Since their maximum strengths at 25 °C under static loading differed, the applied cyclic stresses corresponded to different percentages of their respective maximum strengths. This apparently unorthodox decision for testing strategy was made to facilitate a comparison between the two resin systems in prospective injected connector applications where the SRR would experience identical bearing and splitting stress levels.

LVDTs were used to gauge the splitting deformation of the specimen. The indirect tensile modulus stiffness was acquired by diving the constant force with the accumulated range of horizontal displacement provided by the LVDTs. The stiffness degradation was then calculated at every load cycle as normalised to the initially acquired stiffness i.e., in the first load cycle. Fig. 12 presents the normalised (relative) stiffness, i.e., degradation over the load cycles, of SRR produced with epoxy and UPE + PU resin at a stress level of 7 MPa, corresponding to 70% and 60% of the maximum strength for each resin, accordingly. For the UPE + PU

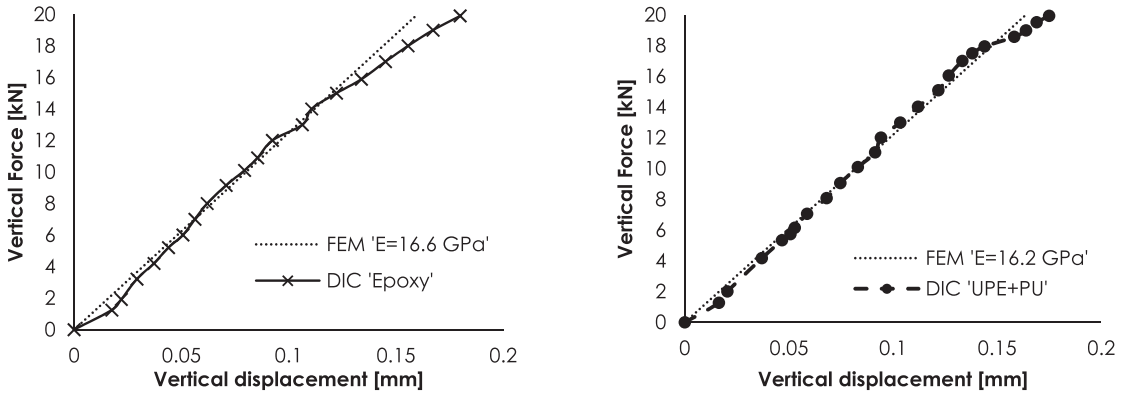

Fig. 10. Vertical displacements close to loading and support points and displacement of test.

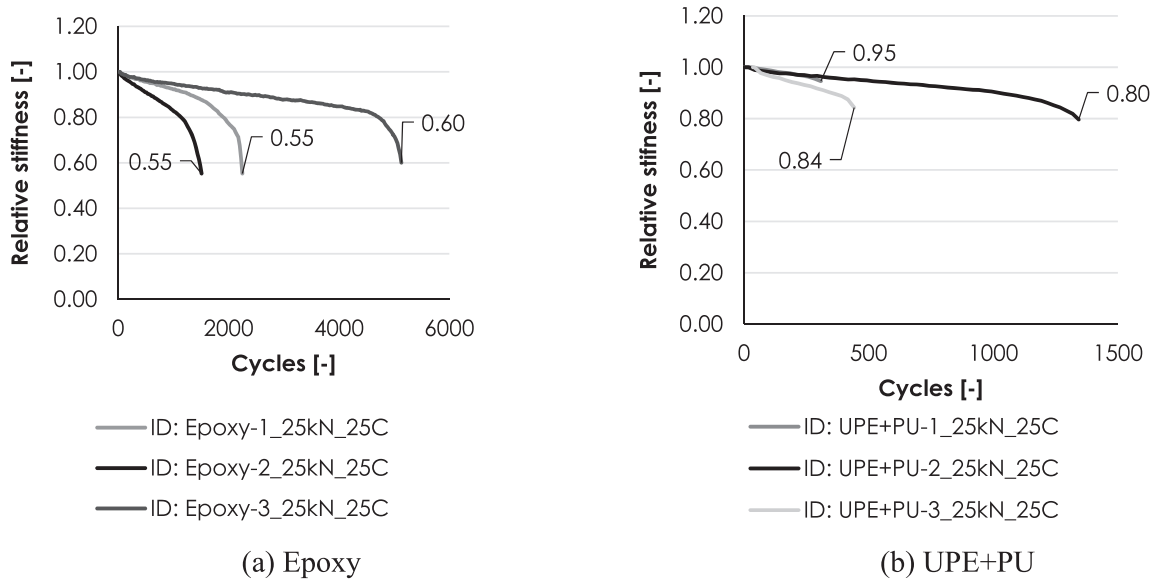

Fig. 12. Normalised stiffness degradation at 25 °C and maximum stress range of 7 MPa (R = 0.1).

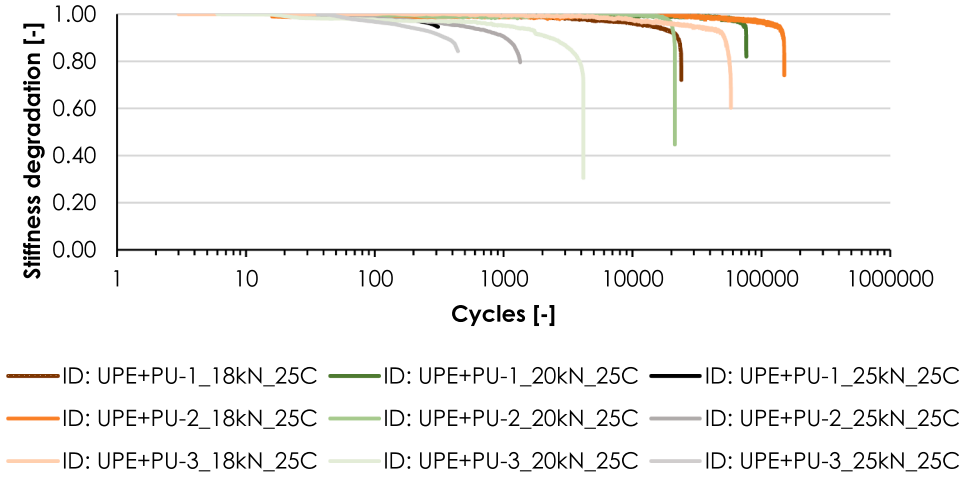

Fig. 13. Normalised stiffness degradation at 25 °C across various load ranges for SRR with UPE + PU.

specimen subjected to this loading scenario, the relative stiffness experienced a gradual reduction until approximately 80% of the fatigue life. Subsequently, the degradation rate accelerated leading to the final brittle fracture of the coupons. In the case of the epoxy resin, an average stiffness degradation of 55% was recorded at the end of the coupons' fatigue life.

For the UPE + PU based SRR disks, the stiffness degradation curves of all nine failed specimens are illustrated in Fig. 13. In this illustration, the black and grey lines designate the tests conducted at 7 MPa while the lowest ranges of 5.55 MPa and 5 MPa are denoted by orange and green colour gradients, respectively. Dispersion of the results is more pronounced under medium stress levels, whereas the results are more consistent for both the lowest and highest loading conditions. On average, a stiffness degradation of approximately 10% was observed before the complete failure of the coupons occurred.

Fatigue performance of the SRR material in the form of stress range versus the number of cycles to failure, the so-called σ-N curves, are constructed and displayed in Fig. 14. Average σ-N curves in Fig. 14 were calculated based on statistical analysis according to the ASTM E729 [39]. This method does not account for runouts i.e., the specimens that did not reach the failure criterion. A linear form was adopted for the double-logarithmic σ-N relationship which is expressed as follows:

$$\log(N) = A + B \bullet \log(S) \tag{3}$$

where N denotes the corresponding number of cycles to failure; S is the stress range endured by the specimen (MPa); and A and B are the regression parameters determined using linear regression. Considering the log(N) and the log(S) as dependent and independent variables, respectively, Equation (3) can be rewritten as:

$$Y = A + B \bullet X \tag{4}$$

The 95% upper and lower confidence bands were not analyzed as the number of coupons would not result in fatigue curves with statistical significance. Nonetheless, the preliminary A and B parameters were determined for both SRRs. Notably, the slope of the σ-N curve was found steeper for the UPE + PU based SRR (B = -14.27) compared to the epoxy variant (B = -17.21), suggesting better fatigue endurance of the epoxy variant. The corresponding A parameters were found equal to 14.79 and 17.78 for the UPE + PU and epoxy resin systems, respectively.

Regarding the failure mode of the investigated SRR systems under indirect tensile cyclic loading, complete splitting of the specimens along the vertical plane was observed for nearly every stress range and across all distinct temperature conditions. However, as previously stated, two epoxy based SRR specimens tested at the lowest stress levels withstood

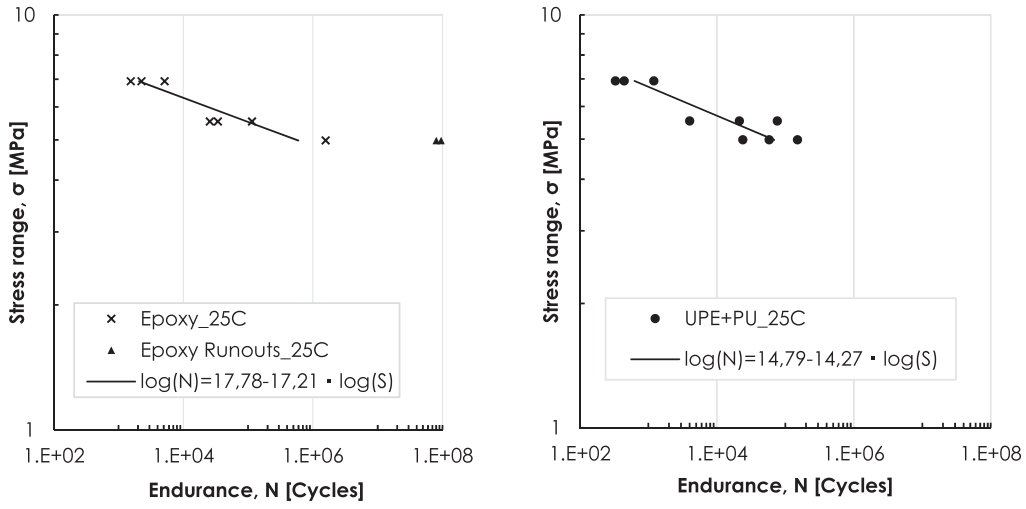

Fig. 14. Preliminary σ-N curves (R = 0.1) for SRR loaded in indirect tensile direction at 25 °C.

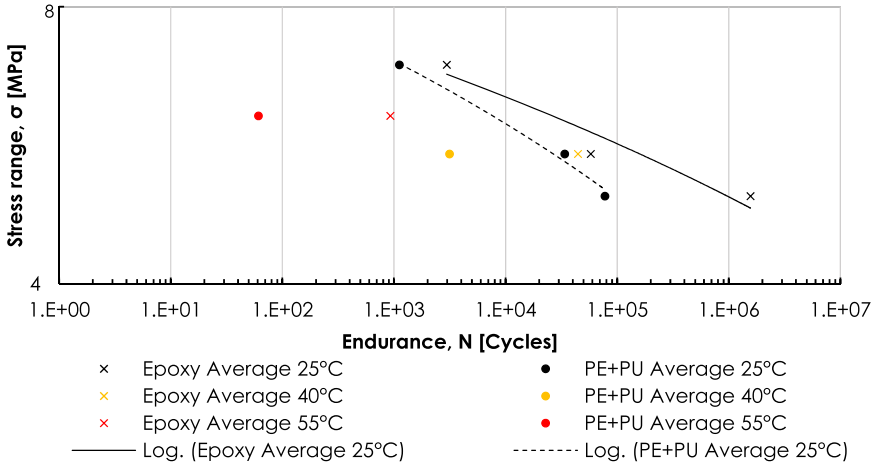

Fig. 15. Endurance of SRR at 25 °C, 40 °C and 55 °C for epoxy and UPE + PU resin systems.

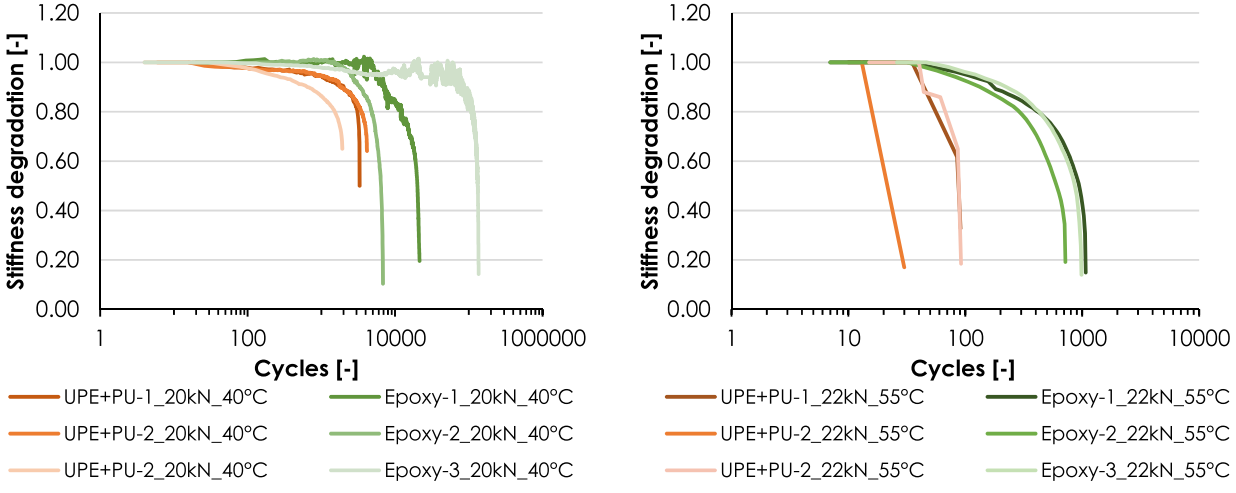

Fig. 16. Normalised stiffness degradation at elevated temperatures.

over 8 million cycles without fracturing or exhibiting plastic deformation. In these instances, localized deformations were observed at the loading strip edges, but no stiffness degradation was recorded.

Additionally, two cyclic load tests were performed under elevated temperature conditions. Stress range of 6.1 MPa was subjected at a temperature of 55 °C, and 5.55 MPa at 40 °C. A collection of the acquired data is provided in Fig. 15, with the average curves obtained previously at room temperature displayed for comparison purposes.

For a stress range equal to 5.55 MPa (48%•$\sigma_{max,epoxy}$, 55%•$\sigma_{max,UPE+PU}$), experimental results for both resins at room and elevated temperature of 40 °C were obtained. In particular, the average value of cycles leading to fracture in the epoxy SRR specimens was determined to be 58,000 and 44,500 at 25 °C and 40 °C, respectively. Conversely, the UPE + PU SRR samples failed after an average of 35,500 cycles at room temperature which reduced by a factor of 10 when the temperature rose to 40 °C, resulting in 3200 cycles. Furthermore, the epoxy based SRR coupons persisted for a minimum of 10 times more cycles to failure compared to the UPE + PU SRR counterparts.

Fig. 16 presents the normalized stiffness degradation curves for tests conducted at both elevated temperatures. With respect to the tests performed at 40 °C, the fatigue endurance of the UPE + PU based SRR samples grouped around 3200 cycles, while the variability among the epoxy resin samples became more pronounced. The UPE + PU resin samples, subjected to testing at 55 °C and a stress range of 6.1 MPa, experienced premature failure which prevented the documentation of their progressive stiffness degradation. The scarcity of input data yielded linear lines, as illustrated in Fig. 16. Conversely, the epoxy based SRR coupons endured, on average, 1000 cycles before failure, with their nonlinear trend effectively captured. Minimal dispersion among the distinct coupons was observed for epoxy based SRR at 55 °C. Thus, epoxy based SRR materials exhibited superior fatigue resistance and durability compared to UPE + PU SRR materials, particularly at elevated temperatures.

4. Water absorption

Water absorption tests were conducted on bulk resin specimens and SRR specimens with two main objectives: to test the saturation levels of different resins and investigate susceptibility to corrosion of the composite steel-polymer system which SRR is. The goal was to assess which resin system could be best for application in injected connectors with a risk of exposure to harsh moisture conditions.

4.1. Water gain of unreinforced resin

Pure resin plates were manufactured using glass molds with Teflon frames. Subsequent to a 24-hours period, the plates were removed from the molds and subjected to a post-curing process at 60 °C for 5 hours in accordance with the material datasheet provided by the resin supplier [30]. Afterward, the resin samples were sectioned into the desired nominal dimensions i.e., cubes of 50x50x4 mm, using a Computer Numerical Control (CNC) cutting machine. These specimens were then used to assess the water uptake by monitoring weight gain over time. Initially, the dried specimens were weighed and then immersed in tap water at various temperatures for six months, during which their weight was recorded at regular intervals. This process involved removing the coupons from the bath, eliminating excess water with a wipe, and returning the samples to the immersion media to continue exposure. The moisture uptake (M_t) for every specimen was calculated using Equation (5):

$$M_t = \left(\frac{w_t - w_0}{w_0}\right) \bullet 100 \quad (5)$$

where w_0, w_t represent the dry stage weight and the weight after a fixed time (t) of exposure to water, respectively.

The experimentally obtained moisture uptake data as a function of the square root of time after six months of exposure are plotted in Fig. 17 for the three types of resin. Each data point represents the mean value of the measured data acquired from three replicated specimens whereas the error bars indicate the standard deviation. Red dashed lines, representing a 1.0% weight gain, have been incorporated as a comparative reference across the diverse resin and SRR systems under investigation. Moreover, the optimal fit for the Fickian diffusion model for each ageing condition was obtained utilizing non-linear curve fitting and is

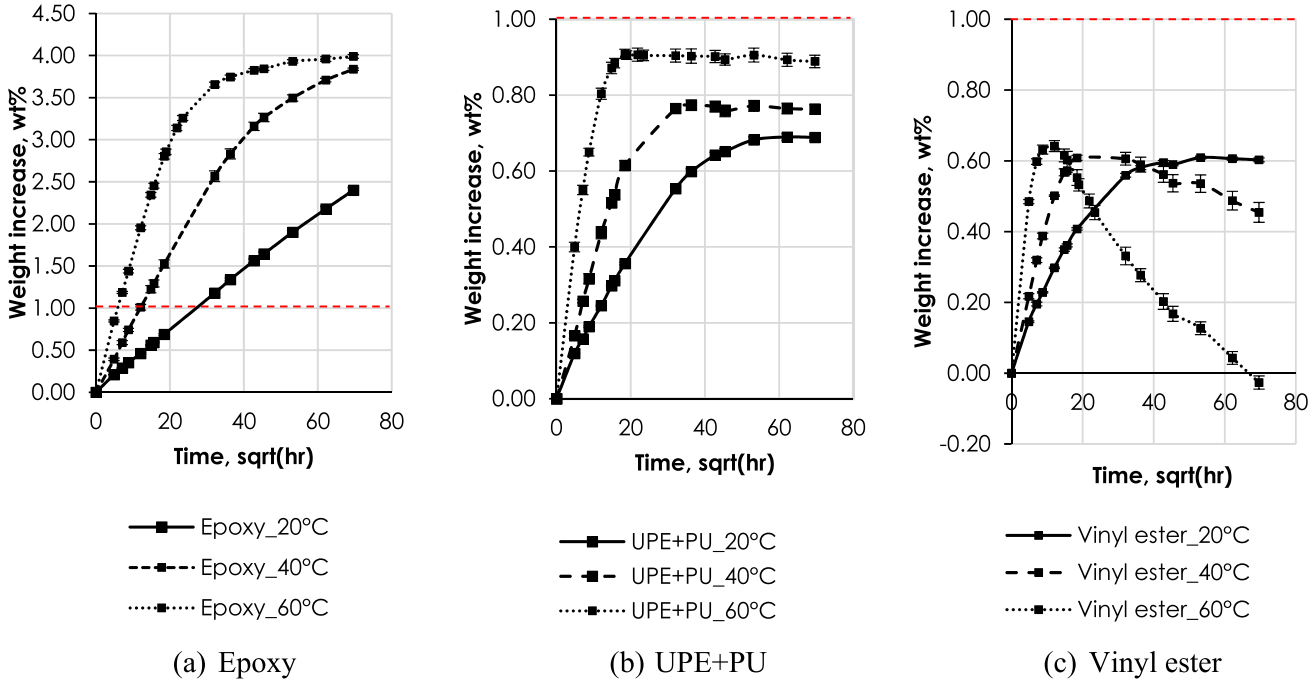

Fig. 17. Weight change of pure resins versus square root of water immersion time, square(t) for temperatures varying from 20 °C to 60 °C (red dashed line included at 1.0% as a reference in all three graphs).

represented by solid or dashed lines, depending on the exposure temperature.

As evidenced by the water absorption profiles presented in Fig. 17, all three hygrothermally exposed resin systems initially gained weight linearly with the square root of time. Higher temperatures appear to accelerate the moisture uptake behaviour and greatly shorten the moisture saturation time. In several instances, saturation was not observed; however, the rate of water gain entered a downward trend due to weight loss. This phenomenon suggests either irreversible water entrapment and degradation of the polymeric structure due to hygrothermal ageing, also reported in [40] or leaching of low molecular weight material into the water phase as in [41]. Nevertheless, no visible damage was observed in the tested samples.

4.2. Water gain of SRR

SRR coupons were also immersed in water, adhering to the same principles employed for the pure resins. The primary deviations from the previous series of tests pertained to coupon production and immersion. Challenges encountered during the sectioning of SRR plates necessitated the adoption of casts with specified dimensions for each coupon, measuring 80x80x8 mm. Steel shot was initially added, followed by resin injection via a syringe, as illustrated in Fig. 18**a**. It was estimated that 20% of the volume was attributed to the resin and the rest was covered by the steel shot. This production method resulted in flat side and bottom surfaces and eliminated air void formation, while also replicating the SRR injection process described in [20,21]. The top surfaces of the coupons were not perfectly smooth and thus they were trimmed. To prevent water penetration due to edge imperfections, all coupons' sides with 80x8 mm dimensions were coated with a thin layer of the same resin utilised in their production, as depicted in Fig. 18**b**. Regarding the time duration of the test, the SRR coupons were exposed to water for 200 days.

The SRR coupons were placed in water compartments sustaining constant temperatures of 20, 40, and 60 °C. Following the same absorption procedure outlined in Section 4.1, the water gain was calculated and the sorption curves of the SRR systems were obtained, as shown in Fig. 19. In this illustration, the red dashed line has been included at 0.2% of weight increase for reference purposes. It is noteworthy that, following 200 days of water exposure, all specimens exhibited continuous water uptake, with no observable indication of saturation. Once again, the epoxy based SRR exhibited the highest weight increase of 0.50% when immersed in a water chamber at 60 °C. The equivalent values for UPE + PU and Vinyl ester resins were 60% and 56% lower, respectively. Increasing the temperature accelerated the absorption of water for all coupons apart from the Vinyl ester resin which displayed a similar response when exposed to water at 40 and 60 °C during the first 27 days of the submerging period.

Additionally, upon examination of the external surfaces of the coupons, it was concluded that the metal balls underwent oxidation when combined with the vinyl ester and the UPE + PE systems. This phenomenon conceivably contributed to an accelerated weight gain, albeit not resulting in exceedingly high values. The edge surfaces of the squared blocks, following 27 days of immersion at the highest and lowest temperature for all three SRR types are presented in Fig. 20. It is apparent that the temperature increase hastened the effect of corrosion. For the epoxy resin, this oxidation was almost inconsiderable for all temperatures despite exhibiting the highest weight increase. Lastly, one of the 80x80 mm surfaces of three different SRR coupons is displayed in Fig. 21. The observed corrosion is notably concentrated around the corners and particularly in regions where the additional thin layer was applied. The potential detrimental effects of this corrosion on the SRR performance remain uncertain.

4.3. Discussion on water absorption results

The water intake of all three types of resins was obtained with and without the inclusion of steel shot. Comparing the epoxy specimens immersed in water at 20 °C, it can be observed that the weight increase was reduced by a factor of 12 when steel shot was included in the resin for the same immersion period i.e., 200 days. Similarly, for the UPE + PU and vinyl ester resin, the inclusion of steel resulted in a reduced weight gain of a factor of 6.5 and 5.5, respectively. This immense reduction in the weight gain between the resin and SRR coupons is attributed to two facts: 1) that the SRR samples included resin only up to 20% of their volume and 2) that presence of steel shot elongates the

(a) Production setup

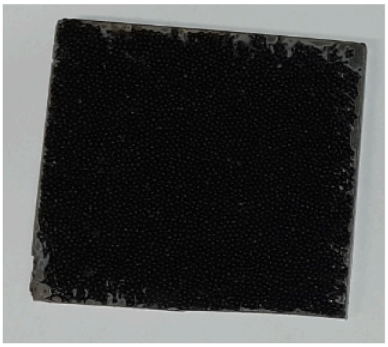

(b) Final product

Fig. 18. SRR coupons for water absorption.

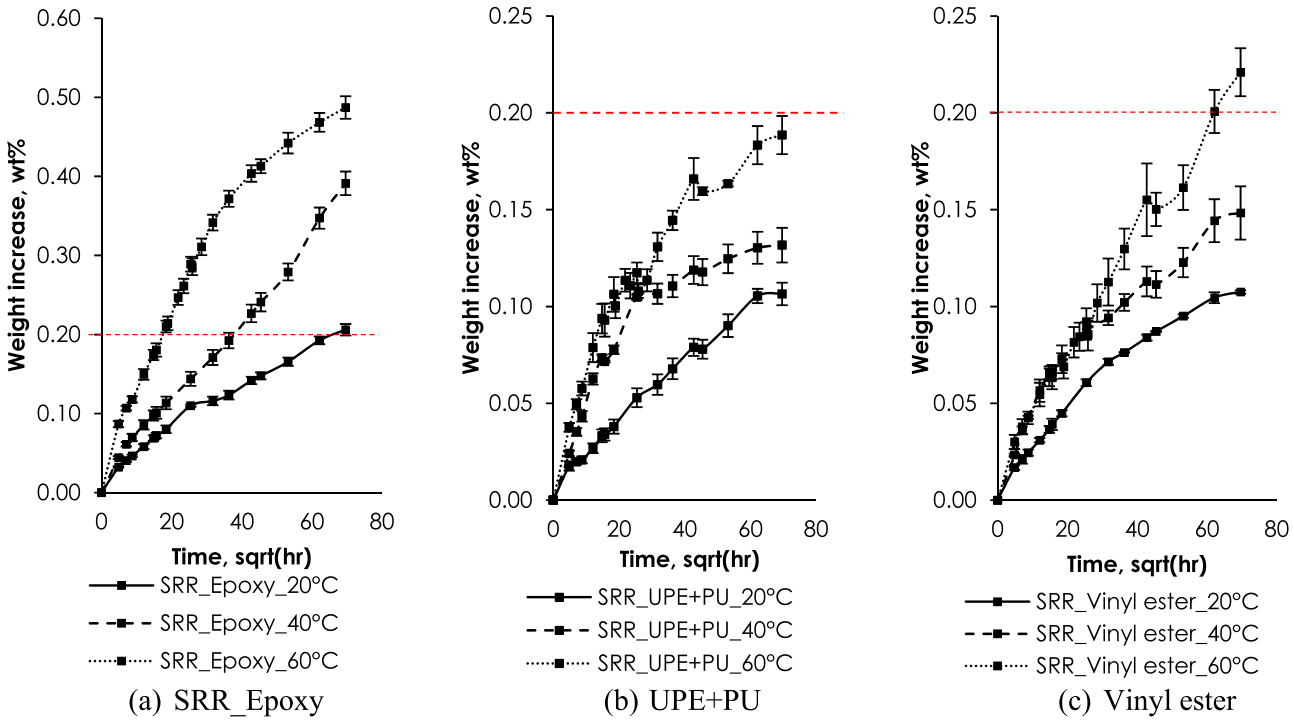

Fig. 19. Weight change of SRR versus square root of water immersion time, square(t) for temperatures varying from 20 °C to 60 °C (red dashed line included at 0.2% as a reference in all three graphs).

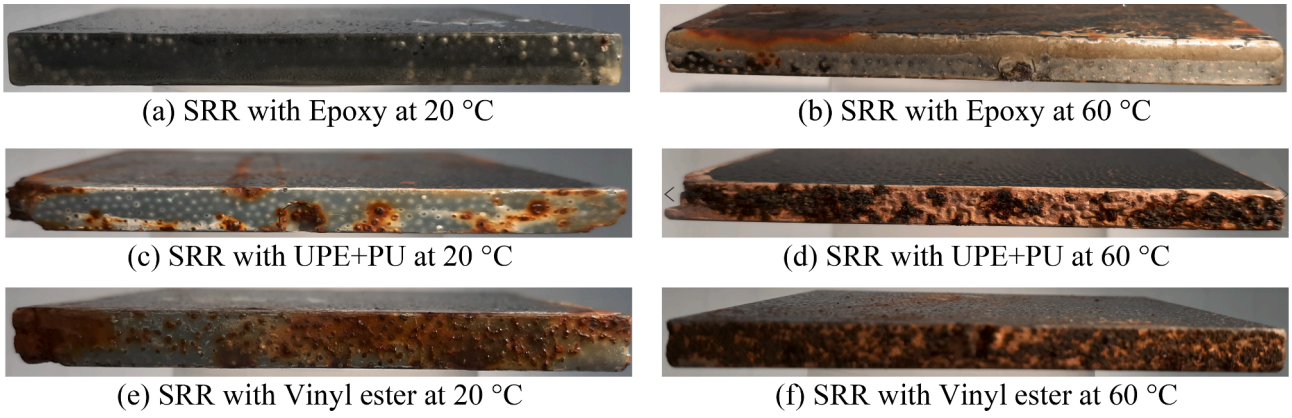

Fig. 20. Edges of SRR specimens after 200 days of immersion at 20 and 60 °C.

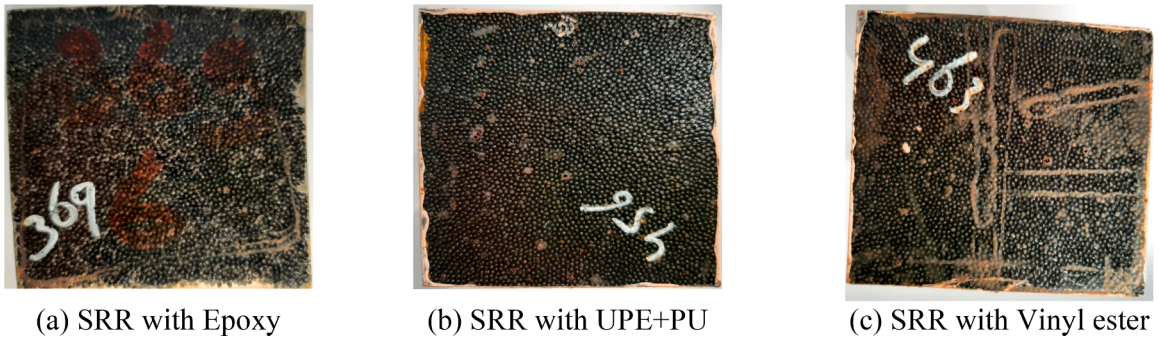

Fig. 21. Top view of SRR specimens after 200 days of immersion at 40 °C.

diffusion path for the water molecules, thus slowing down the diffusion process (note that reinforced resin coupons did not reach saturation). Thus, the integration of steel shot within the resin matrix provides advantages in relation to water absorption profiles and it seems to be more beneficial for the epoxy resin.

Concerning the corrosion susceptibility of the steel balls when embedded in a resin system, it can be concluded that increased water gain does not directly correlate with an increased predisposition for corrosion. Despite the pure epoxy resin exhibiting the most significant water absorption, no corrosion was observed in the epoxy based SRR samples when immersed in water. In contrast, the SRRs with UPE + PU and vinyl ester displayed considerable corrosion at the edges of coupons, despite their relatively low water uptake. Given that the steel balls employed in fabricating the coupons were of consistent quality, suggests that epoxy resin may possess superior metal adhesion properties compared to the UPE + PU and vinyl ester resins investigated in this study.

5. Conclusions

Three different types of resins with T_g values exceeding 110 °C were used to fabricate unreinforced coupons and coupons reinforced with steel shot resin coupons. Steel Reinforced Resin (SRR) disks with D100x23 mm geometry and cube specimens of 80x80x8 mm, featuring a volume fraction of steel balls equal to 80%, were created to determine their strength, modulus, Poisson ratio, σ-N curves, and water absorption profiles under varying temperature conditions. The static and fatigue performance of the SRR was assessed through a series of cylinder splitting tests that are relevant for granular materials such as bituminous asphalt, concrete, or rocks. The water uptake of the pure resin systems was obtained by immersing coupons of 50x50x4 mm in water compartments at 20, 40, and 60 °C. Susceptibility to corrosion of the steel shot within SRR made of three different resins in submerged condition is compared. The following conclusions can be deduced:

1. The maximum tensile splitting strength of SRR made with epoxy was found equal to 11.6 MPa at 25 °C. A lower value of 10.0 MPa and 6.8 MPa was obtained for UPE + PU and vinyl ester resin, accordingly. The tensile moduli of SRR at room temperature were equal to 16.6 GPa, 16.2 GPa, and 14.7 GPa for epoxy, UPE + PU and vinyl ester resin, respectively. The Poisson ratio of the SRR coupons made with epoxy and UPE + PU resin was found equal to 0.13.
2. The indirect tensile strength of the vinyl ester resin exhibited negligible sensitivity to elevated temperatures. In contrast, the respective strength reduction for epoxy and UPE + PU resin at 55 °C was 15% and 25%, respectively. The epoxy resin displayed the greatest sensitivity of tensile modulus to temperature increase, with a 21% modulus decrease observed at 55 °C.
3. Regarding fatigue endurance, the SRR coupons fabricated with epoxy resin withstood 1.6 million cycles at a stress range of 5 MPa, which is approximately 20 times greater than the cycles to failure observed with UPE + PU resin. Preliminary slopes of the S-N curves were determined to be m = -15 for UPE + PU and m = -18 for epoxy resin.
4. The pure epoxy resin, despite exhibiting superior mechanical properties, demonstrated a peak (saturated) water uptake of 4% following 200 days of water immersion at 60 °C. In contrast, the pure UPE + PU and vinyl ester resins experienced maximum weight increases of merely 0.90% and 0.65% respectively, after the same duration of water absorption. The incorporation of steel shot contributed to a reduction in water intake both in terms of saturation level and diffusion rate. After 200 days of water immersion at 20 °C, the SRR coupons fabricated with epoxy resin exhibited the highest water gain percentage, amounting to 0.20%, which is 12 times lower than that obtained from pure epoxy resin coupons. Similarly, the UPE + PU and vinyl ester resins reduced their water gain by factors of 6.5 and 5.5, respectively, resulting in water gains of 0.65% and 0.60% after 200 days of immersion at 20 °C. Notably, the impact of oxidation on the SRR surface was exclusively evident along the edges of the SRR cubic specimens fabricated with either vinyl ester or UPE + PU systems.

CRediT authorship contribution statement

Angeliki Christoforidou: Writing – original draft, Visualization, Validation, Software, Methodology, Investigation, Formal analysis, Data curation, Conceptualization. **Ron Verleg:** Visualization, Resources, Investigation, Data curation. **Marko Pavlovic:** Writing – review & editing, Supervision, Project administration, Methodology, Investigation, Funding acquisition, Conceptualization.

Declaration of Competing Interest

The authors declare that they have no known competing financial interests or personal relationships that could have appeared to influence the work reported in this paper.

Data availability

Data will be made available on request.

Acknowledgements

The authors are very grateful to Rijkswaterstaat, the Dutch Ministry of Infrastructure, for supporting the research. We are equally appreciative of the dedicated staff at the Pavement Lab in the Stevin II Laboratory at TU Delft. Their expertise, willingness to assist, and provision of state-of-the-art equipment greatly contributed to the success of our experimental campaign.

References

[1] P. Zuo, A.P. Vassilopoulos, Review of fatigue of bulk structural adhesives and thick adhesive joints, Int. Mater. Rev. 66 (5) (2020) 313–338.
[2] T.H. Courtney, J. Wulff, Matrix-Limited Fatigue Properties in Fibre Composite Materials, Mater. Sci. 1 (4) (1966) 333–388.
[3] G. Tao, Z. Xia, Biaxial fatigue behavior of an epoxy polymer with mean stress effect, Int. J. Fatigue 31 (4) (2009) 678–685.
[4] Broughton, W. and R. Mera, *Review of durability test methods and standards for assessing long term performance of adhesive joints.* NPL REPORT CMMT (A)61, 1997.
[5] E. Hagerup, Flexural fatigue testing of polyesters, Appl. Polym. Sci. 7 (1963) 1093–1116.
[6] R.W. Hertzberg, J.A. Manson, Environment, Frequency and Temperature Effects on Fatigue in Engineering Plastics, in: J.J. Burke, V. Weiss (Eds.), Fatigue, Springer US, Boston, MA, 1983, pp. 231–240.
[7] L.J. Broutman, S.K. Gaggar, Fatigue Behavior of Epoxy and Polyester Resins, Int. J. Polym. Mater. Polym. Biomater. 1 (4) (2006) 295–316.
[8] J. Brunbauer, G. Pinter, Effects of mean stress and fibre volume content on the fatigue-induced damage mechanisms in CFRP, Int. J. Fatigue 75 (2015) 28–38.
[9] I. Constable, J.G. Williams, D.J. Burns, Fatigue and cyclic thermal softening of thermoplastics, Mech. Eng. Sci. 12 (1) (1970) 20–29.
[10] F.M.G. Ramírez, M.F.S.F. Moura, R.D.F. Moreira, F.G.A. Silva, A review on the environmental degradation effects on fatigue behaviour of adhesively bonded joints, Fatigue Fract. Eng. Mater. Struct. 43 (7) (2020) 1307–1326.
[11] F. Ascione, et al., Hygrothermal durability of epoxy adhesives used in civil structural applications, Compos. Struct. 265 (2021), 113591.
[12] F. Ascione, L. Granata, A. Lombardi, The influence of the hygrothermal aging on the strength and stiffness of adhesives used for civil engineering applications with pultruded profiles: an experimental and numerical investigation, J. Adhes. 98 (12) (2022) 1733–1771.
[13] M. Savvilotidou, A.P. Vassilopoulos, M. Frigione, T. Keller, Development of physical and mechanical properties of a cold-curing structural adhesive in a wet bridge environment, Constr. Build. Mater. 144 (2017) 115–124.
[14] S. Gantayat, D. Rout, S.K. Swain, Carbon Nanomaterial-Reinforced Epoxy Composites: A Review, Polym.-Plast. Technol. Eng. 57 (1) (2017) 1–16.
[15] D.R. Bortz, C. Merino, I. Martin-Gullon, Carbon nanofibers enhance the fracture toughness and fatigue performance of a structural epoxy system, Compos. Sci. Technol. 71 (1) (2011) 31–38.
[16] T. Adachi, M. Osaki, W. Araki, S.-C. Kwon, Fracture toughness of nano- and micro-spherical silica-particle-filled epoxy composites, Acta Mater. 56 (9) (2008) 2101–2109.

[17] C.M. Manjunatha, A.C. Taylor, A.J. Kinloch, S. Sprenger, The effect of rubber micro-particles and silica nano-particles on the tensile fatigue behaviour of a glass-fibre epoxy composite, J. Mater. Sci. 44 (1) (2009) 342–345.
[18] Nijgh, M.P., *New Materials for Injected Bolted Connections - A Feasibility Study for Demountable Connections*. 2017, Delft University of Technology.
[19] Nijgh, M.P., *A multi-scale approach towards reusable steel-concrete composite floor systems*. 2021, Delft University of Technology.
[20] G. Olivier, F. Csillag, E. Tromp, M. Pavlović, Conventional vs. reinforced resin injected connectors' behaviour in static, fatigue and creep experiments on slip-resistant steel-FRP joints, Eng. Struct. 236 (2021) 112089.
[21] F. Csillag, M. Pavlović, Push-out behaviour of demountable injected vs. blind-bolted connectors in FRP decks, Compos. Struct. 270 (2021) 114043.
[22] G. Olivier, et al., Feasibility of bolted connectors in hybrid FRP-steel structures, Constr. Build. Mater. 383 (2023), 131100.
[23] M.P. Nijgh, H. Xin, M. Veljkovic, Non-linear hybrid homogenization method for steel-reinforced resin, Constr. Build. Mater. 182 (2018) 324–333.
[24] B. Pedrosa, L. Bücking, M. Veljkovic, Eng. Struct. 256 (2022) 114023.
[25] Csillag, F., *Demountable deck-to-girder connection of FRP-steel hybrid bridges*. 2018, Delft Technical University.
[26] B. Gómez-Meijide, I. Pérez, G. Airey, N. Thom, Stiffness of cold asphalt mixtures with recycled aggregates from construction and demolition waste, Constr. Build. Mater. 77 (2015) 168–178.
[27] A. Afshar, M. Alkhader, C.S. Korach, F.-P. Chiang, Effect of long-term exposure to marine environments on the flexural properties of carbon fiber vinylester composites, Compos. Struct. 126 (2015) 72–77.
[28] T. Jeffrey Hsu, L. James Lee, Physical properties of transfer-molded polyurethane-polyester, Appl. Polymer Sci. 33 (1987) 793–807.
[29] S.G. Damani, L. James Lee, The resin-fiber interface in polyurethane and polyurethane-unsaturated polyester, Polym. Compos. 11 (3) (1990).
[30] Datasheet Resoltech 1080S - Highest Performance Epoxy Laminating & Infusion System. 2016.
[31] *Datasheet Daron 8151*.
[32] *Datasheet ATLAC 430*. 2018.
[33] G. Cerni, E. Bocci, F. Cardone, A. Corradini, Correlation Between Asphalt Mixture Stiffness Determined Through Static and Dynamic Indirect Tensile Tests, Arab. J. Sci. Eng. 42 (3) (2017) 1295–1303.
[34] T. Ma, N. Peng, Z. Zhu, Q. Zhang, C. Yang, J. Zhao, Brazilian Tensile Strength of Anisotropic Rocks: Review and New Insights, Energies 11 (2) (2018) 304.
[35] ASTM, *Standard Test Method for Splitting Tensile Strength of Cylindrical Concrete Specimens*. Designation: C 496 – 96, 2017.
[36] EN, *Bituminous mixtures - Test methods for hot mix asphalt - Part 26: Stiffness*. European Committee for Standardization, 2012.
[37] R.A. Stirling, D.J. Simpson, C.T. Davie, The application of digital image correlation to Brazilian testing of sandstone, Int. J. Rock Mech. Min. Sci. 60 (2013) 1–11.
[38] Y. Belrhiti, J.C. Dupre, O. Pop, A. Germaneau, P. Doumalin, M. Huger, T. Chotard, Combination of Brazilian test and digital image correlation for mechanical characterization of refractory materials, J. Eur. Ceram. Soc. 37 (5) (2017) 2285–2293.
[39] ASTM, *E739 10 Standard Practice for Statistical Analysis of Linear or Linearized Stress-Life* 1980, Annual Book of ASTM Standards.
[40] G.Z. Xiao, M.E.R. Shanahan, Water absorption and desorption in an Epoxy Resin with degradation, Centre National de la Recherche Scientifique (1996).
[41] X. Yin, Y. Liu, Y. Miao, G. Xian, Water Absorption, Hydrothermal Expansion, and Thermomechanical Properties of a Vinylester Resin for Fiber-Reinforced Polymer Composites Subjected to Water or Alkaline Solution Immersion, Polymers (Basel) 11 (3) (2019) 505.